



Contents lists available at ScienceDirect

Sensors and Actuators: B. Chemical

journal homepage: www.elsevier.com/locate/snbImproved ppb-level NO₂ conductometric sensor induced by trace Au on SnO₂ nanosheetWeiyi Bu^a, Yan Zhang^a, Qixuan Qin^a, Yuliang Li^a, Xiaohong Chuai^{a,*}, Zhijie Zhou^b, Changhua Hu^b, Tianshuang Wang^a, Peng Sun^a, Fangmeng Liu^a, Geyu Lu^{a,*}^a State Key Laboratory of Integrated Optoelectronics, Key Laboratory of Advanced Gas Sensors, Jilin Province, College of Electronic Science and Engineering, International Center of Future Science, Jilin University, 2699 Qianjin Street, Changchun 130012, China^b High-Tech Institute of Xi'an, Xi'an 710025, Shaanxi Province, China

ARTICLE INFO

Keywords:

SnO₂ nanosheet aggregates
Au loaded
NO₂ gas sensor
Ppb-level
UV light-assisted reduction method

ABSTRACT

As a main exhaust emission from vehicles, nitrogen dioxide is harmful to environment and human health. Gas sensors with high performance for nitrogen dioxide detection is essential. In this work, SnO₂ nanosheet aggregates loaded with Au were used to fabricate a NO₂ gas sensor. Pristine SnO₂ was synthesized via a solvothermal method. Subsequently, the ultraviolet (UV) light-assisted reduction method was utilized to load Au nanoparticles and improve the sensing properties. The SnO₂ modified with a trace of Au nanoparticles (0.5 wt%) shows high response to ppb-level NO₂ (35–100 ppb) at a low temperature (90 °C). Besides excellent selectivity and long-term stability, the 0.5% Au/SnO₂ based sensor can detect 2 ppb NO₂ with the response value of 1.2. The enhanced sensing properties can be attributed to the interface interaction between Au and SnO₂, causing the enhanced absorption capability for oxygen and NO₂ molecules. Additionally, trace amount of loading Au can maintain small size of Au nanoparticles, making the active sites on SnO₂ more effective. This work provides a convenient method for preparing a ppb-level NO₂ gas sensor with high performance.

1. Introduction

Nitrogen dioxide (NO₂) is the main exhaust emission from vehicles, aggravating the formation of acid rain and photochemical smog with the surge of vehicles in these years [1,2]. Undesirable consequences such as the reduction of atmospheric visibility [3], acidification of surface water [4], potential eutrophication [5] and the increasing content of toxins in waters can be witnessed. Besides the damage to environment, NO₂ can cause direct harm to human health. Even low concentration of NO₂ (53 ppb) may increase the incidence of acute respiratory diseases in children as announced by the US Environmental Agency [6]. Therefore, it is essential to monitor the concentration of NO₂ in our surrounding environment.

There are a few technologies to detect NO₂, including gas chromatography [7], electrochemistry method [8] and spectrophotometer [9], but their shortcomings, such as the complicated operation steps and bulky volume limit their widespread application. However, gas sensors made of metal oxide semiconductor (MOS) have attracted researchers'

attention in recent years because of their low cost, miniaturization and intriguing sensing performance [10,11]. NO₂ sensors based on typical MOS, including n-type semiconductors (SnO₂ [6,12,13], In₂O₃ [14,15]) and p-type semiconductors (NiO [16,17], CuO [1,18]), have been fabricated. Among them, n-type SnO₂ with a wide band of 3.59 eV is a potential material for detecting NO₂ [19]. However, the sensing performances of pure SnO₂ based gas sensors cannot completely satisfy the application requirement, especially selectivity and limit of detection (LOD) remaining problems to be solved. Several methods have been reported to improve the properties of gas sensing materials. Among them, noble metal (Au, Ag, Pd and Pt et al.) loading is an effective method, because noble metal nanoparticles have high catalytic activity [20–27]. Yu et al. fabricated H₂S sensor based on Pt-decorated ZnO nanorods and the obtained LOD was as low as 1.1 ppb [25]. Zhao et al. prepared Pd-In₂O₃ to detect methane and proved the significantly improved sensing properties with Pd loading [26]. Saito et al. prepared Au-loaded pyramid-shaped ZnO particles with a response value of 1371–1 ppm isoprene, which was 45 times higher than that of pristine

* Corresponding authors.

E-mail addresses: xhchuai@jlu.edu.cn (X. Chuai), luyg@jlu.edu.cn (G. Lu).¹ fax: +86-431-85167808<https://doi.org/10.1016/j.snb.2022.133237>

Received 14 August 2022; Received in revised form 29 November 2022; Accepted 23 December 2022

Available online 24 December 2022

0925-4005/© 2022 Elsevier B.V. All rights reserved.

ZnO particles [21]. Wang et al. synthesized ZnO flowers functionalized by Au nanoparticle with outstanding sensing performance to acetone [24].

In this work, a trace of Au nanoparticles loaded SnO₂ was used to fabricate a NO₂ sensor. Compared to the pure SnO₂, the Au/SnO₂ exhibited higher sensitivity and faster response to ppb-level NO₂, especially reduced the LOD to 2 ppb. The effect brought about by Au nanoparticles was evaluated via multiple characterization methods. The increased concentration of oxygen vacancy and improved NO₂ adsorption property are attributed to the interface interaction between Au and SnO₂. The ameliorative NO₂ sensing performance was also given reasonable explanation.

2. Experimental section

All the chemical reagents used were analytically pure, they are listed in Table S1 in the Supplementary data.

2.1. Preparation of sensing materials

2.1.1. Preparation of SnO₂ nanosheet aggregates

In a typical preparation process, 2 mmol tin chloride dihydrate (SnCl₂·2 H₂O), 1 mmol hexamethylene tetramine (C₆H₁₂N₄) and 10 mmol sodium hydroxide (NaOH) were dissolved into a mixture solution with 20 mL of deionized water and 20 mL of absolute alcohol. The above solution was stirred for 90 min, and then transferred into a Teflon-lined stainless-steel autoclave and heated at 180 °C for 18 h. After cooling down to RT naturally, the solid precipitates were collected by centrifugation and washed with deionized water and ethanol several times. After being dried in 80 °C for 12 h, the obtained powder was annealed at 500 °C for 3 h in a muffle furnace (heating rate was 1 °C min⁻¹).

2.1.2. Preparation of Au/SnO₂ nanosheet aggregates

Typically, 100 mg of the obtained SnO₂ powder was dispersed in ethanol and magnetically stirred. Then, a certain amount of HAuCl₄ aqueous solution (0.01 M) was added. Its mass ratios to SnO₂ were respectively 0.3%, 0.5%, and 1.0% for three samples. The solution was irradiated by ultraviolet (UV) light ($\lambda = 365$ nm, 10 mW/cm²) for 5 min at room temperature with stirring. For comparison, another 0.5% Au/SnO₂ (S) was also obtained by impregnation reduction method. Sodium borohydride (NaBH₄) as well as HAuCl₄ were added into the SnO₂ aqueous suspension and stirred for 90 min. Subsequently, the Au/SnO₂ product was centrifuged with deionized water several times and dried for several hours. Finally, the collected powder was calcined at 400 °C for 2 h in a muffle furnace (heating rate was 1 °C min⁻¹). The synthetic

process is schematically illustrated in Fig. 1.

2.2. Characterization

X-ray powder diffraction (XRD Rigaku D/Max 2550) with Cu K α radiation ($\lambda = 0.15418$ nm) was used to analyze the crystalline phases of samples. The angle scanning range was from 20° to 70°. The field-emission scanning electron microscopy (FESEM JEOL JSM-7500 F) was utilized to observe the samples' morphologies, operated at an acceleration voltage of 10 kV, the attached energy dispersive X-ray spectrometry (EDS) was adopted to investigate the samples' elemental composition. The morphology details of the samples were obtained by transmission electron microscopy (TEM; JEOL JSM-2100 F) and high-resolution transmission electron microscopy (HRTEM; JEOL JSM-2100 F). To analyze the surface composition and element valence, X-ray photoelectron spectra (XPS) were carried out with Al K α as the excitation source and corrected with respect to the standard peak of C 1s at 284.3 eV. The desorption properties of the materials to NO₂ were measured by the NO₂ temperature programmed desorption (NO₂-TPD, AMI-300, USA) with a mass spectrometer for gas analysis (Omnistar, Pfeiffer, Germany).

2.3. Sensor fabrication and property testing

The schematic illustration of a chemiresistive gas sensor is shown in Fig. S1. Its fabrication process and measurement method on gas sensing were detailedly described in our previous work [28,29]. For the device fabrication, the mixture of sample powder and ethanol was made into slurry in an agate mortar and brushed uniformly onto a ceramic tube having a pair of gold electrodes at its two ends. To control the operating temperature of a sensor, a Ni-Cr alloy coil heater was inserted through the ceramic tube. Resistances of the as-fabricated device in air or target gas were measured by using a multimeter (Fluke 8864 A), whose maximum range is up to 1 G Ω . The traditional static testing system was adopted, different NO₂ concentration was obtained by diluting different volume of standard NO₂ gas with air in 1 L of the gas chamber. The sensitivity is defined as $S = R_a/R_g$ for reducing gas or $S = R_g/R_a$ for oxidizing gas, where R_a and R_g are the resistances in air and in certain test gas atmosphere, respectively. Gas response and recovery time are defined as the time required for 90% of the total resistance change throughout adsorption and desorption process. The effect of humidity on sensing performance was studied. The various relative humidity was set at 25 °C by using the humidity chamber (Shanghai ESPC Environment Equipment Corporation, China).

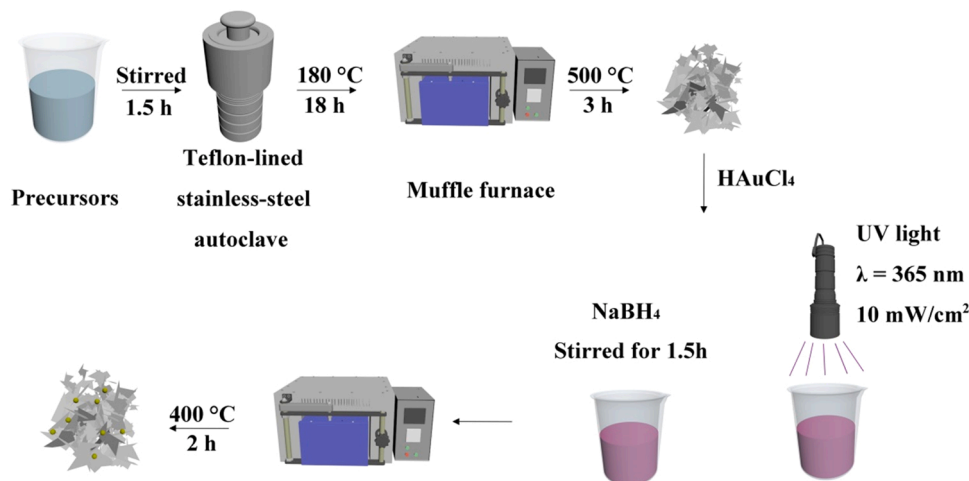


Fig. 1. Schematic diagram of the preparing process of Au loaded SnO₂.

3. Results and discussion

3.1. Characterization of the Samples

To investigate the phase information of the samples, the powder XRD patterns of the pristine SnO₂, 0.3% Au/SnO₂, 0.5% Au/SnO₂, 0.5% Au/SnO₂ (S) and 1.0% Au/SnO₂ were measured and shown in Fig. 2 (a). For the first four samples, their diffraction peaks can be completely matched with those of rutile SnO₂ (JCPDS PDF 41-1445) without extra characteristic diffraction peaks from Au. For 1.0% Au/SnO₂, an additional peak at around 44.5° (Fig. 2 (b)), which corresponds to (200) diffraction of Au (JCPDS PDF 1-1174) can be observable. The increased loading amount of Au for 1.0% Au/SnO₂ brings about the detectable signal from Au.

The FESEM images of pure SnO₂, 0.3% Au/SnO₂, 0.5% Au/SnO₂, 0.5% Au/SnO₂ (S) and 1.0% Au/SnO₂ are presented in Fig. S2. It can be seen that all these SnO₂ samples are made up of nanosheet aggregates with the size of a few microns. Au loading does not have significant effect on the morphology of SnO₂. And the Au particles could be only discerned from FESEM pictures of 0.5% Au/SnO₂ (S) and 1.0% Au/SnO₂ (Fig. S2 (h) and Fig. S2 (j)). The contents of Au were analyzed by EDS (Fig. S3) and listed in Table S2, which are roughly consistent with desired results. To explore the detailed microstructure, the TEM and HRTEM images of all samples were obtained (Fig. 3, Fig. S4 and Fig. S5). The samples are composed of aggregated nanosheets, in agreement with their FESEM images. For Au loaded SnO₂, Au nanoparticles with distinct contrast can be apparently observed on the surface of the nanosheets. The size of Au nanoparticles is about 8–10 nm for 0.3% Au/SnO₂ and 0.5% Au/SnO₂. Their HRTEM images (Fig. 3 (c) and Fig. S4 (f)) further show the lattice spacing of 0.235 nm and 0.335 ± 0.001 nm, corresponding to the (111) lattice plane of Au and (110) lattice plane of SnO₂, respectively. But for 1.0% Au/SnO₂, the dimension of the Au nanoparticles is roughly 40 nm (Fig. S4 (g-i)), indicating the agglomeration of Au with the increasing amount of added HAuCl₄. As for 0.5% Au/SnO₂ (S), different sizes (10–60 nm) of Au nanoparticles can be observed, exhibiting the size inhomogeneity by impregnation reduction method (Fig. S5 (a-c)). Also, the elemental mapping images of 0.5% Au/SnO₂ (Fig. 3 (d-g)) and 0.5% Au/SnO₂ (S) (Fig. S5 (d-g)) describe the even dispersion of Sn, O, and Au elements throughout the sample. The above results verify that the Au nanoparticles are loaded on the SnO₂ nanosheets.

The surface atomic compositions and element chemical state of the samples were analyzed by X-ray photoelectron spectroscopy (XPS). The corresponding spectra of all the samples are shown in Fig. 4. All the signals from Sn, O, C and Au can be observed from their full spectra (Fig. 4 (a)). For pristine SnO₂, the peaks of Sn 3d_{3/2} and 3d_{5/2} are located at 494.53 and 486.13 eV (Fig. 4 (b)). However, with the amount

of loaded Au increasing, these characteristic peaks shifted in the direction of high binding energy (Sn 3d_{3/2}: from E (SnO₂) = 494.53 eV to E (1.0% Au/SnO₂) = 494.93 eV; Sn 3d_{5/2}: from E (SnO₂) = 486.13 eV to E (1.0% Au/SnO₂) = 486.48 eV). This implies that electron density of Sn⁴⁺ in outer shell decreases by interaction of Au with SnO₂. The high resolution XPS of Au 4f electron is shown in Fig. 4 (d). The binding energy at around 83.20 and 86.85 eV, is attributed to 4f_{7/2} and 4f_{5/2}, respectively. Their energy positions are little lower than 84.00 and 87.71 eV of metallic Au [30,31], which is opposite to the above of Sn 3d XPS spectra. Combining the XPS spectra of Sn and Au, it is inferred that there exists electron transfer from SnO₂ to Au, which might be caused by the difference between their work functions. Additionally, the high-resolution spectra of O 1s (Fig. 4 (c)) for all the samples can be fitted into three characteristic peaks, which are related to three kinds of oxygen species. The peaks at 529.8 ± 0.30, 530.8 ± 0.30, 532.2 ± 0.30 eV are attributed to the lattice oxygen (O_L), deficient oxygen (O_V) and surface-adsorbed oxygen (O_C), respectively [11]. The percentages of these oxygen species are listed in the Table S2. It shows that 0.5% Au/SnO₂ has the highest ratio of O_V/O_L and O_C/O_L among all the Au loaded SnO₂ samples.

The NO₂ temperature programmed desorption (NO₂-TPD) curves of pure SnO₂ and 0.5% Au/SnO₂ were measured and compared (Fig. 5). As seen from them, there are several peaks which are related with desorption of two different nitrate species [32]. The start-up temperatures for desorption of pure SnO₂ and 0.5% Au/SnO₂ are about 80 °C. Meanwhile, the area under TPD curve is a little larger for 0.5% Au/SnO₂, presenting higher amount of adsorbed NO₂ molecules caused by more active sites. The above results verify the interfacial interaction between Au nanoparticles and SnO₂ has a positive effect on the NO₂ absorption properties.

3.2. Sensing performance

The responses of all these sensors based on pristine SnO₂, 0.3% Au/SnO₂, 0.5% Au/SnO₂ and 1.0% Au/SnO₂ toward 100 ppb NO₂ were measured at different operating temperature (Fig. 6 (b)). It can be seen that as the temperature goes up, the response values of the four sensors increase firstly and then decrease. The maximum response values for all sensors locate consistently at 90 °C. The relationship of response versus operating temperature was also discussed in pervious literature [30]. Compared to the pure SnO₂, Au-loaded SnO₂ shows a higher response to 100 ppb NO₂ at 90 °C. Among them, 0.5% Au/SnO₂ shows the maximum value of 35, which is 8.2 times higher than that of the pure SnO₂ (3.8). Continuing to increase Au content sharply decreases the response. The resistance values of the Au-loaded SnO₂ in fresh air also change because of Au loading. As shown in Fig. 6 (a), the Au-loaded SnO₂ samples

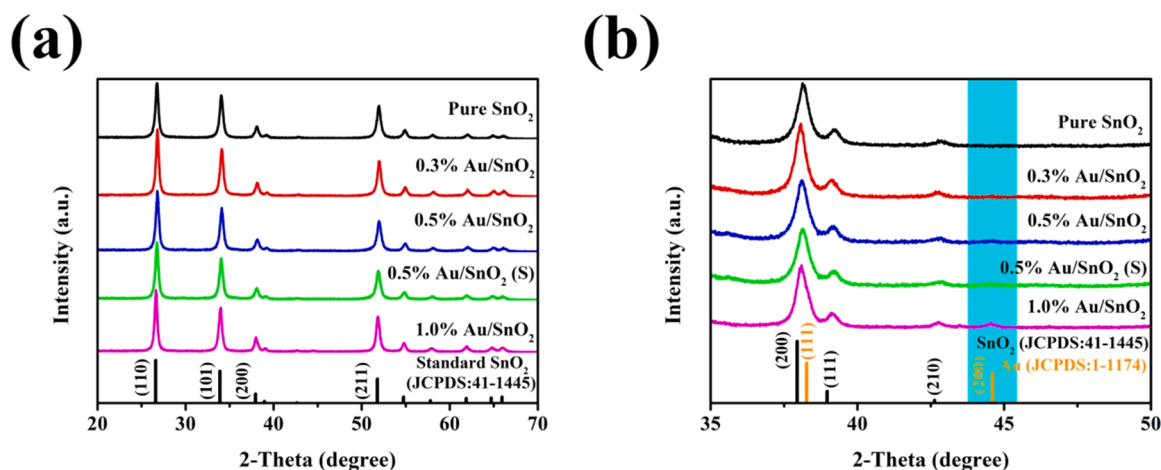


Fig. 2. (a) XRD patterns of the Au loaded SnO₂ samples with different Au loading amount. (b) Comparison of partial peaks from XRD spectra.

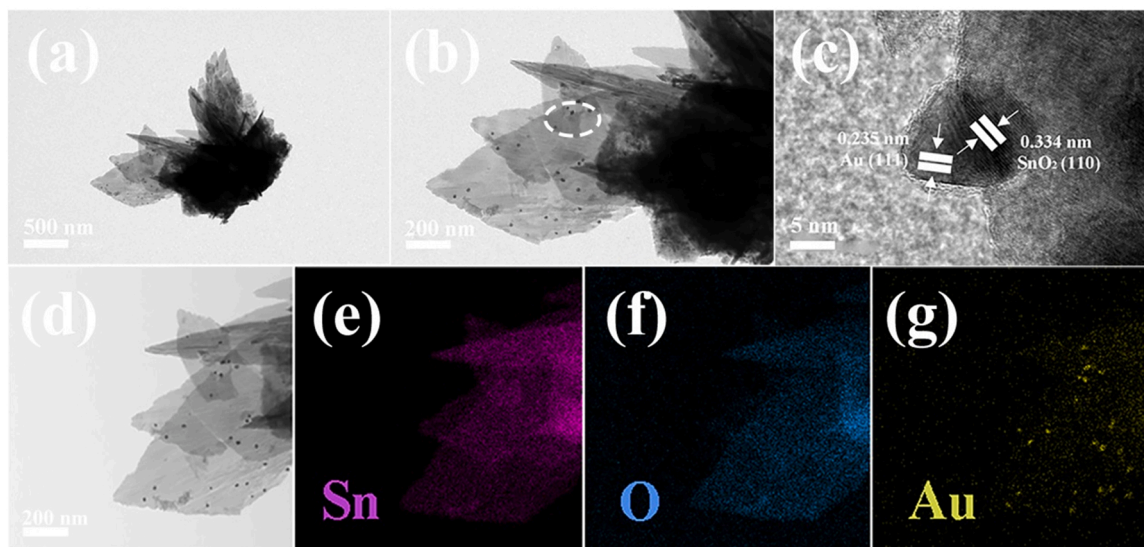


Fig. 3. (a, b) TEM and (c) HRTEM images; (d-g) sample and corresponding elemental mapping images of Sn, O and Au, respectively for 0.5% Au/SnO₂ sample.

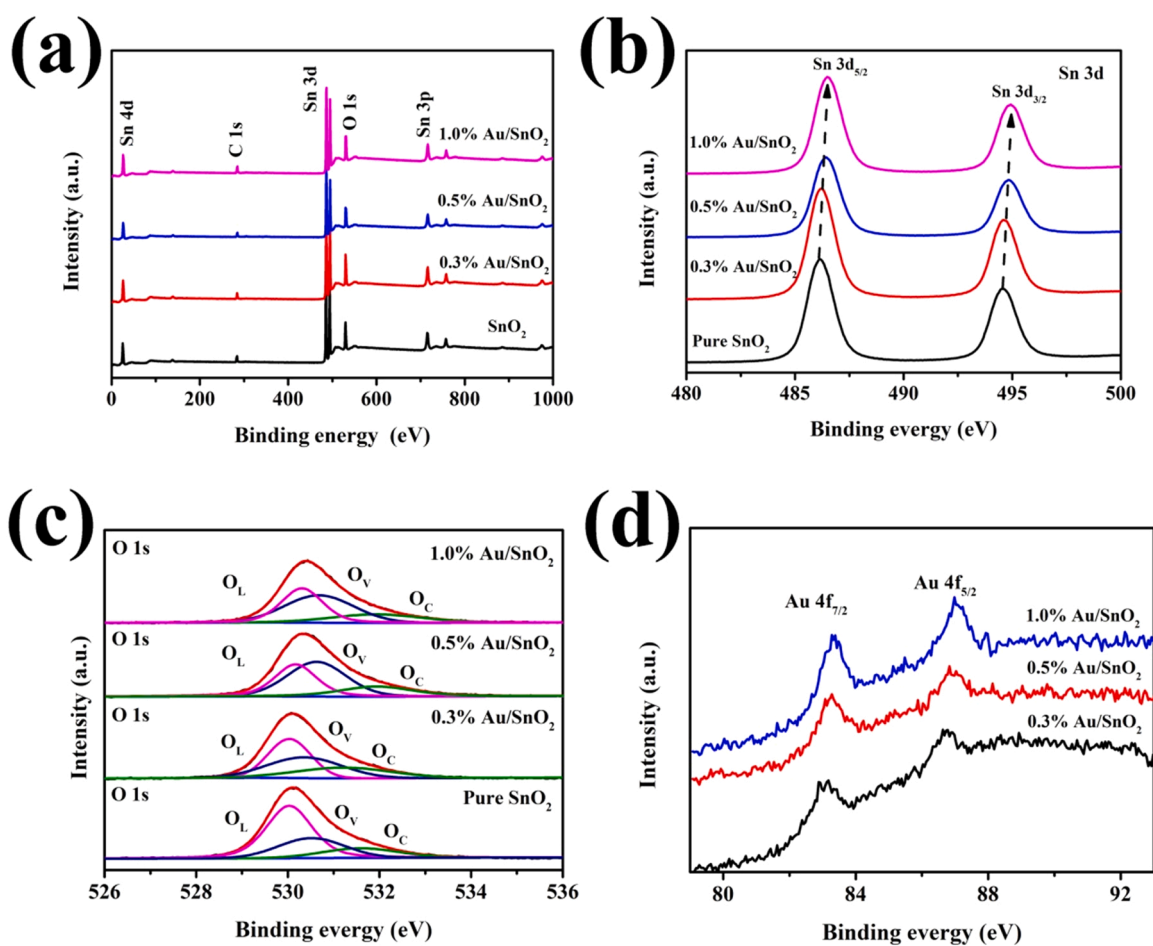


Fig. 4. XPS spectra of the samples: (a) full range, (b) Sn 3d (c) O 1 s, and (d) Au 4 f.

exhibit better conductivity than pristine SnO₂ and the 0.5% Au/SnO₂ has the lowest resistance. Deficient oxygen can be the main causes for it. For these samples, it is noteworthy that the concentration of oxygen vacancy, electric resistant and response value to NO₂ have the same change trend with increasing amount of loaded Au. Au nanoparticles with small size and well distribution are vital to this phenomenon.

Furthermore, the responses of the 0.5% Au/SnO₂ based sensor to various gases, including NO₂, CO, SO₂, NH₃, benzene, acetone, toluene and ethanol at 90 °C are compared in Fig. 6 (c). The respective concentration of NO₂, CO, SO₂ and NH₃ is 1 ppm, while it is 100 ppm for other VOCs. As seen for it, the response to NO₂ is far higher than those to the other gases by two orders of magnitude. It can be concluded that the 0.5%

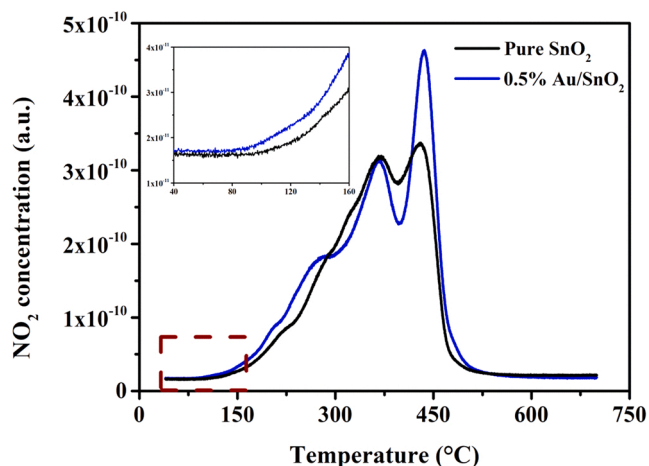


Fig. 5. NO₂ temperature-program desorption (TPD) curves of pure SnO₂ and 0.5% Au/SnO₂.

Au/SnO₂ based sensor exhibits super selectivity toward NO₂ over these interference gases.

The relationship between response values of the sensors and gas concentration was investigated. Fig. 6 (d) provides the fitting function curves of pure SnO₂ and 0.5% Au/SnO₂ based sensors under different concentrations of NO₂ gas (20–1000 ppb). For these two sensors, it can be represented empirically by the function of $\text{Log}(S-1) = a\text{Log}C + b$,

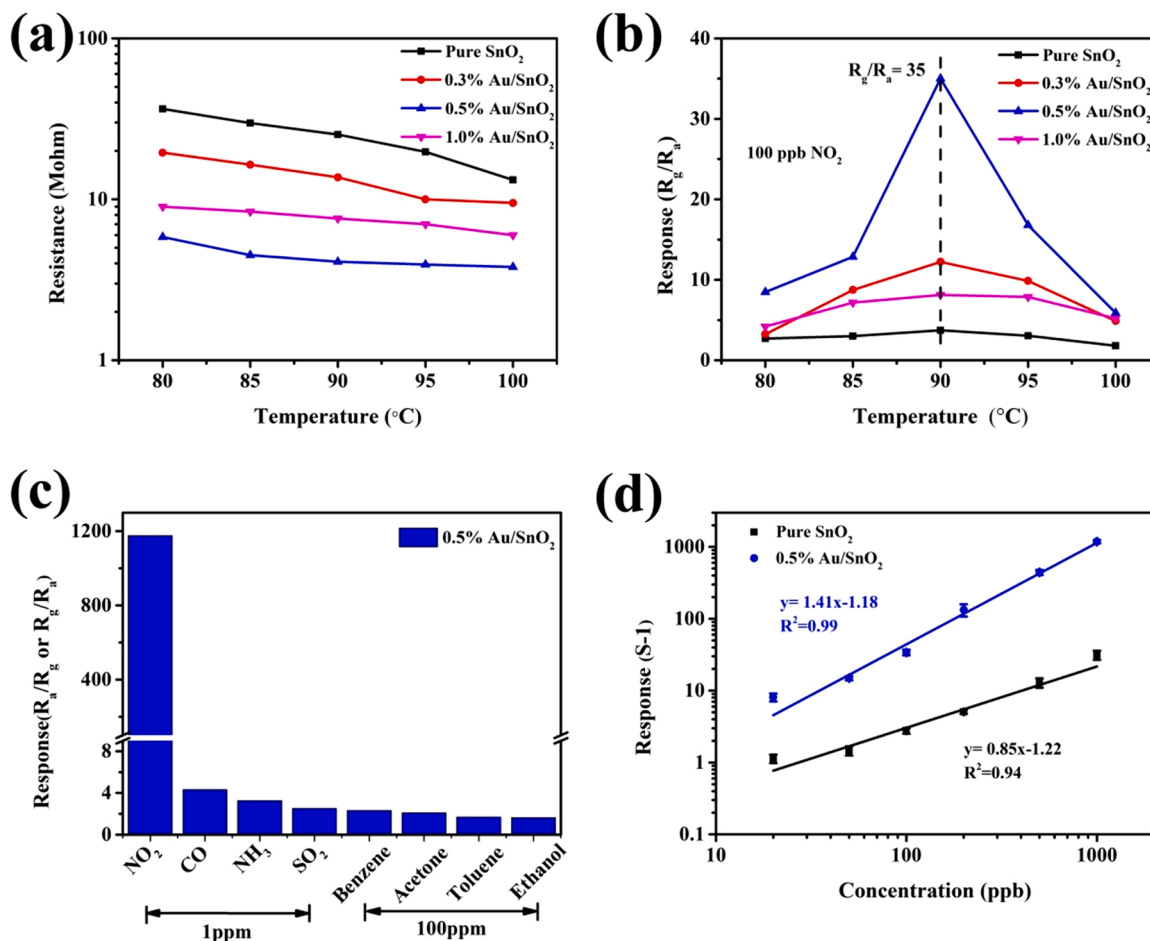


Fig. 6. (a) Resistance values of sensors based on Au loaded SnO₂ samples with different Au loading amount in fresh air at various temperatures; (b) The responses of sensors to 100 ppb NO₂ at different operating temperatures; (c) Responses of 0.5% Au/SnO₂ based sensor to various gases at 90 °C; (d) The fitting function curves of pure SnO₂ and 0.5% Au/SnO₂ based sensors under different concentrations of NO₂ gas (20–1000 ppb).

which S and C represents the sensor response and NO₂ concentration, respectively [33]. The slope of 0.5% Au/SnO₂ (1.41) is higher than that of pure SnO₂ (0.85), indicating a more promising sensing performance for detecting NO₂ [34]. In addition, 0.5% Au/SnO₂ based sensor have more excellent linearity ($R^2 = 0.99$) in logarithmic form than pure SnO₂ ($R^2 = 0.94$), illustrating the 0.5% Au/SnO₂ are more suitable to be used as sensing material in practical application [35]. Meanwhile, the transient response curve of the 0.5% Au/SnO₂ based sensor to 100 ppb NO₂ is shown in Fig. 7 (a). Compared to pure SnO₂ (Fig. S6), it displays faster response/recovery to NO₂. The response/recovery time of the 0.5% Au/SnO₂ based sensor is 484/286 s, while it is 740/2295 s for pure SnO₂. The dynamic response curves and response/recovery time of the 0.5% Au/SnO₂ based sensor with 20, 50, 100 and 200 ppb concentration of NO₂ were recorded (Fig. S7). The recovery time decreases with NO₂ concentration. It is not the case for response time. Given the high resistance value, which is beyond the upper measurement limit of Fluke 8864 A (1 G Ω) at NO₂ concentration higher than 200 ppb, the resistance was measured by using resistance meter SM-8213 (HIOKI). The dynamic process cannot be displayed at this situation.

To explore the LOD of the 0.5% Au/SnO₂ based sensor, the performance to several ppb NO₂ is investigated and the dynamic response curves are shown in Fig. 7 (b), 2 ppb NO₂ can be detected with the response value of 1.2. The corresponding response value versus NO₂ concentration is plotted in Fig. S8. It is worth emphasizing that simulated air was used in place of ambient air in the testing system to eliminate the impacts of NO₂ in air and ensure the correct detection at very low concentration of NO₂. Also, the dynamic response curves with

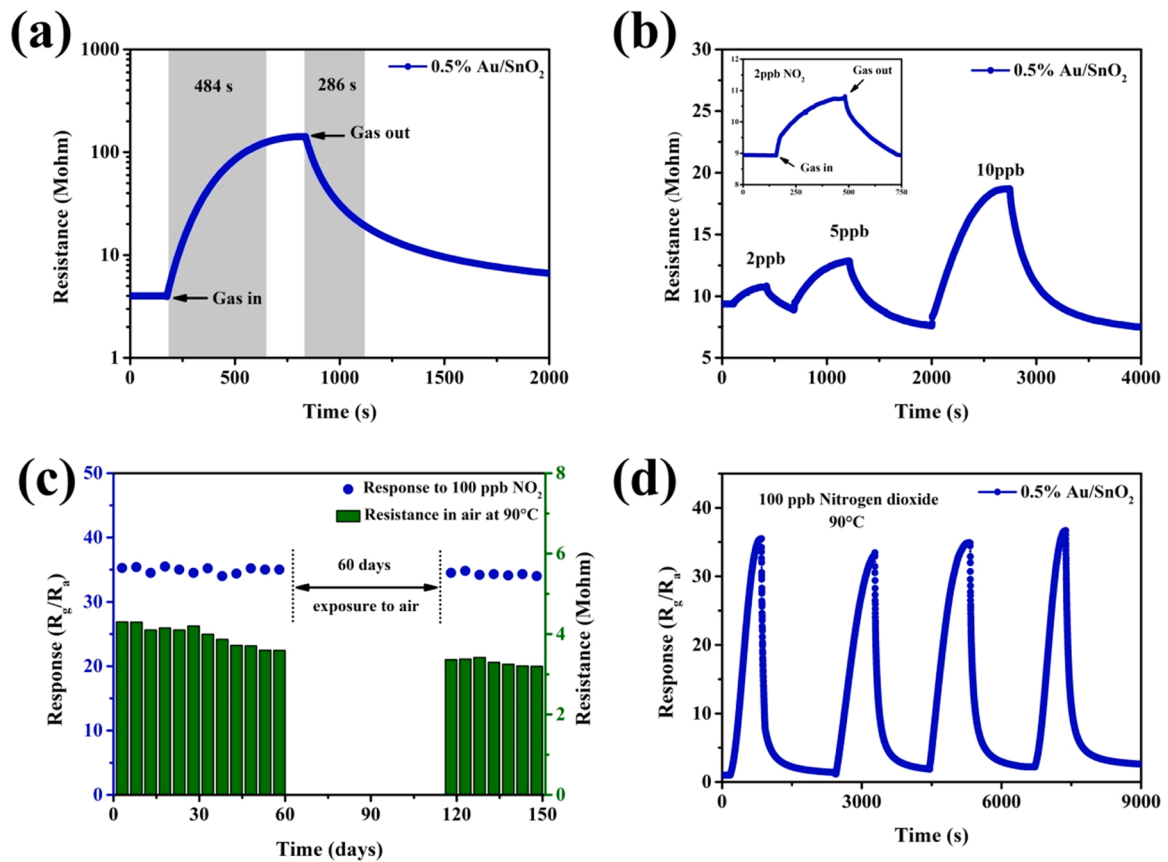


Fig. 7. (a) Transient curve of 0.5% Au/SnO₂ based sensor at 90 °C to 100 ppb NO₂; (b) The dynamic response curves of 0.5% Au/SnO₂ based sensor to NO₂ in low concentration (2–10 ppb), the insert shows the transient response curve to 2 ppb NO₂ (the LOD); (c) Long-term stability of 0.5% Au/SnO₂ based sensor to 100 ppb NO₂ at 90 °C in 150 days; (d) Four-cycle test curve of 0.5% Au/SnO₂ based sensor to 100 ppb NO₂.

20, 50, 100 ppb concentration of NO₂ were recorded in Fig. S9. It can be seen that the response to different concentration of NO₂ in simulated air has an unobvious increase compared to that in ambient air. Also, the sensor displayed a tardier response/recovery without the interaction with water molecules. Additionally, long-term stability is a necessary factor for evaluating the sensing performance. The sensor based on 0.5% Au/SnO₂ was tested within 150 days. Its steady responses to 100 ppb NO₂ in Fig. 7 (c) exhibited its outstanding long-term stability. Good repeatability is also manifested in four cycle measurement (Fig. 7 (d)).

The influence of humidity on sensing performance should be considered in practical application. So, the transient response curves of 0.5% Au/SnO₂ based sensor to 100/200 ppb NO₂ at 90 °C were measured in various relative humidity (RH) (15%, 30%, 45%, 60%, 75%

and 90%) (Fig. S10). As shown in Fig. 8 (a, b), both the response to NO₂ and resistance values in air decrease with the humidity increasing. Compared to the response values in 30% RH (routine humidity condition in testing system), a reduction of 31.4% to 100 ppb and 24.8% to 200 ppb in 90% RH were measured. This phenomenon may be explained by the process of active sites being poisoned with hydroxyl groups [36–38]. At high humidity, more water molecules occupy the adsorption sites on the surface of Au/SnO₂, impeding the adsorption of NO₂ molecules and reducing the response value. Moreover, response/recovery kinetics of the fabricated sensor are also affected by humidity (Fig. 8 (c)). The response time decreases from 484 s at 30% RH to 257 s at 90% RH and recovery time reduces from 286 s to 62 s. Such results might be attributed to the increased electronic conductivity caused by the interaction of SnO₂ with water molecule. The enhanced interaction between

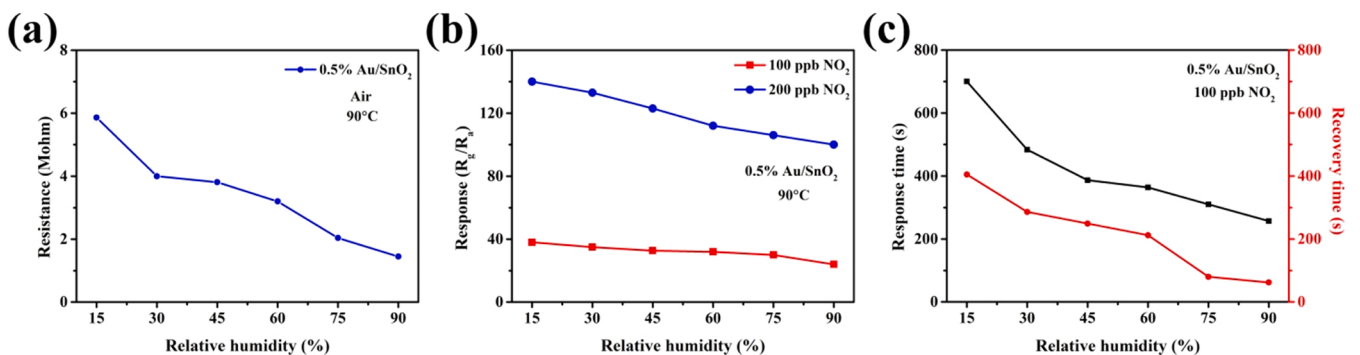


Fig. 8. (a) Resistance value in air, (b) response value and (c) response/recovery time of 0.5% Au/SnO₂ based sensor to 100/200 ppb NO₂ at various humidity (The setting temperature at humidity chamber was 25 °C).

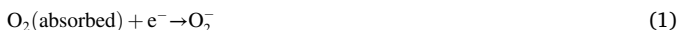
water vapor and the target gas may also be one reason [39–41].

In order to compare the effect on the sensing performance of Au loaded SnO₂ with different reduction methods, the response values of 0.5% Au/SnO₂ (S) to NO₂ were investigated (Fig. S11). Under 100 ppb NO₂, the maximum response value is 17 at 90 °C, which is higher than that of pristine SnO₂ but lower than that of 0.5% Au/SnO₂, indicating that the gas sensing properties of the Au loaded SnO₂ obtained by different reduction methods are quite different [42]. The enhanced performance of Au loaded SnO₂ obtained by UV irradiation could be due to its uniform and appropriate Au nanoparticle size.

To appraise the sensing properties of 0.5% Au/SnO₂ to NO₂, other NO₂ sensors reported in the literature are listed in Table S3 and their sensing performances are compared. Among these devices, the 0.5% Au/SnO₂ based sensor exhibits high response to ppb-level NO₂ and the low LOD.

3.3. Sensing Mechanism

For a chemiresistive gas sensor, it is well accepted that adsorbed oxygen molecules play an important part in sensing process. They can capture electrons from the conduction band of sensing material and be ionized into O₂⁻ (lower than 150 °C) [6]. When the sensor contacts with oxidative NO₂ atmosphere, chemical reaction between the adsorbed NO₂ molecules and active O₂⁻ occurs with electrons involved [43]. The dissipated electrons from sensing material in this process bring about the increase of resistance. The above sensing mechanism is schematically illustrated in Fig. 9 and the involved sensing reactions are expressed in Eqs. (1)–(3) [44]:



In our work, 0.5% Au/SnO₂ exhibits far higher response and faster response/recovery speed to NO₂ than pristine SnO₂. Obviously, loaded Au can be responsible for the performance enhancement. According to the analysis on element XPS, it is manifested that the concentration of oxygen vacancy increases for Au/SnO₂ samples compared to pure SnO₂. Among them, 0.5% Au/SnO₂ has the maximum oxygen vacancy

concentration. Oxygen vacancy acts as an active site for oxygen absorption and is conducive to sensing process. It is reasonable that 0.5% Au/SnO₂ exhibits the highest response to NO₂ among these sensors. Besides, small size of Au nanoparticles may be another cause [45]. Appropriate amount of Au nanoparticles with small size can highlight its spillover sensitization. This is the case for 0.5% Au/SnO₂. On the contrary, large Au particle in 1.0% Au/SnO₂ weakens its spillover effect. Additionally, NO₂-TPD curves confirm that, 0.5% Au/SnO₂ occupies better absorption ability to NO₂. It is the case that the sensitivity characteristic is greatly ameliorated for 0.5% Au/SnO₂ based sensor. This result verifies the effect of Au loading on NO₂ adsorption. In addition, Schottky contact can be formed between Au and SnO₂. The work function of Au (5.1 eV) is larger than that of SnO₂ (4.9 eV) [46,47], and the band diagram is shown in Fig. S12. Co-electron flows from SnO₂ to Au until equilibrium of their Fermi energy. The formation of depletion layer at SnO₂ side may contribute to improved sensitivity of SnO₂, but the phenomenon about the decrease in resistance of the Au/SnO₂ comparing to pure SnO₂ is dominated by the concentration of oxygen vacancy. On the whole, the interfacial reaction between SnO₂ and Au brings about comprehensive effect enhancing the NO₂ sensing performance of SnO₂.

4. Conclusions

Based on Au loaded SnO₂ nanosheet aggregates, a highly selective and sensitive NO₂ sensor was fabricated. It has a high response of 35–100 ppb NO₂ at a low operating temperature (90 °C), and the LOD can reach 2 ppb. Combined characterization results with measurement, the factors for the enhanced sensing property are investigated and analyzed. Apart from spillover effect and electron sensitization, the additional interfacial interaction between Au and SnO₂ may play an important role. This reaction brings about improved oxygen vacancy concentration and NO₂ absorption capability. The relative high concentration of oxygen vacancy provides more active sites for the selective adsorption reaction, endowing the Au/SnO₂ sensors with high sensitivity and good selectivity to NO₂ at a low operating temperature. The modulated NO₂ absorption property may make contribute to the sensitivity of 0.5% Au/SnO₂ based sensor. Overall, this work provides a facile method for preparing high-performance NO₂ sensors by loading trace amounts of Au on the SnO₂ nanosheets.

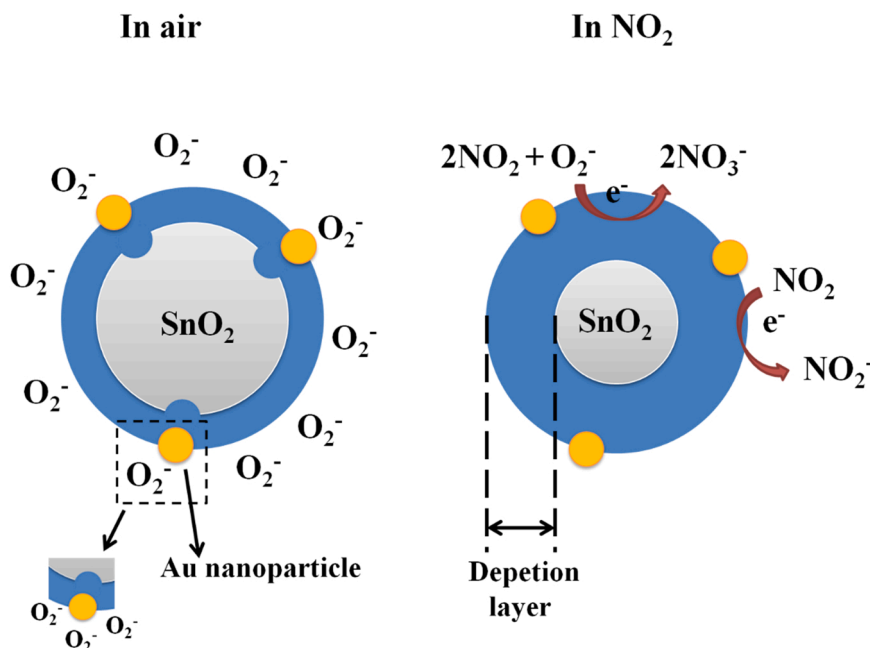


Fig. 9. Schematic illustration of the sensing mechanism.

CRedit authorship contribution statement

Weiyi Bu: Conceptualization, Methodology, Writing – original draft, Validation, Writing – review & editing. **Yan Zhang:** Resources, Investigation, Writing – review & editing. **Qixuan Qin:** Formal analysis, Writing – review & editing. **Yuliang Li:** Methodology, Writing – review & editing. **Xiaohong Chuai:** Conceptualization, Methodology, Resources, Project administration, Funding acquisition, Writing – review & editing. **Zhijie Zhou:** Methodology, Writing – review & editing. **Changhua Hu:** Methodology, Writing – review & editing. **Tianshuang Wang:** Conceptualization, Methodology, Writing – review & editing. **Peng Sun:** Methodology, Writing – review & editing. **Fangmeng Liu:** Methodology, Writing – review & editing. **Geyu Lu:** Conceptualization, Resources, Supervision, Project administration, Funding acquisition, Writing – review & editing.

Declaration of Competing Interest

The authors declare that they have no known competing financial interests or personal relationships that could have appeared to influence the work reported in this paper.

Data availability

Data will be made available on request.

Acknowledgments

This work is supported by the key project of the National Natural Science Foundation of China (No. 61833016, 62033002).

Appendix A. Supporting information

Supplementary data associated with this article can be found in the online version at [doi:10.1016/j.snb.2022.133237](https://doi.org/10.1016/j.snb.2022.133237).

References

- J. Hu, C. Zou, Y. Su, M. Li, Y. Han, E.S.-W. Kong, Z. Yang, Y. Zhang, An ultrasensitive NO₂ gas sensor based on a hierarchical Cu₂O/CuO mesocrystal nanoflower, *J. Mater. Chem. A* 6 (2018) 17120–17131.
- W. Liu, L. Xu, K. Sheng, C. Chen, X. Zhou, B. Dong, X. Bai, S. Zhang, G. Lu, H. Song, APTES-functionalized thin-walled porous WO₃ nanotubes for highly selective sensing of NO₂ in a polluted environment, *J. Mater. Chem. A* 6 (2018) 10976–10989.
- M. Hollaway, O. Wild, T. Yang, Y. Sun, W. Xu, C. Xie, L. Whalley, E. Slater, D. Heard, D. Liu, Photochemical impacts of haze pollution in an urban environment, *Atmos. Chem. Phys.* 19 (2019) 9699–9714.
- J. Zhang, X. Gao, Nutrient distribution and structure affect the acidification of eutrophic ocean margins: A case study in southwestern coast of the Laizhou Bay, China, *Mar. Pollut. Bull.* 111 (2016) 295–304.
- J. Wang, T. Feng, J. Chen, V. Ramalingam, Z. Li, D.M. Kabtamu, J.H. He, X. Fang, Electrocatalytic nitrate/nitrite reduction to ammonia synthesis using metal nanocatalysts and bio-inspired metalloenzymes, *Nano Energy* 86 (2021), 106088.
- L. Meng, Y. Li, M. Yang, X. Chuai, Z. Zhou, C. Hu, P. Sun, F. Liu, X. Yan, G. Lu, Temperature-controlled resistive sensing of gaseous H₂S or NO₂ by using flower-like palladium-doped SnO₂ nanomaterials, *Microchim. Acta* 187 (2020) 297.
- H. Zhao, A.G. Dana, Z. Zhang, W.H. Green, Y. Ju, Experimental and modeling study of the mutual oxidation of N-pentane and nitrogen dioxide at low and high temperatures in a jet stirred reactor, *Energy* 165 (2018) 727–738.
- S.M. Ahn, D.Y. Kim, J. Suk, Y. Kang, H.K. Kim, D.W. Kim, Mechanism for preserving volatile nitrogen dioxide and sustainable redox mediation in the nonaqueous lithium-oxygen battery, *ACS Appl. Mater. Interfaces* 13 (2021) 8159–8168.
- H. Diémoz, A.M. Siani, S. Casadio, A.M. Iannarelli, G.R. Casale, V. Savastoiouk, A. Cede, M. Tiefengraber, M. Mueller, Advanced NO₂ retrieval technique for the Brewer spectrophotometer applied to the 20-year record in Rome, Italy, *Earth Syst. Sci. Data* 13 (2021) 4929–4950.
- W. Jiang, L. Meng, S. Zhang, X. Chuai, Z. Zhou, C. Hu, P. Sun, F. Liu, X. Yan, G. Lu, Design of highly sensitive and selective xylene gas sensor based on Ni-doped MoO₃ nano-pompon, *Sens. Actuators B: Chem.* 299 (2019), 126888.
- L. Meng, W. Bu, Y. Li, Q. Qin, Z. Zhou, C. Hu, X. Chuai, C. Wang, P. Sun, G. Lu, Highly selective triethylamine sensing based on SnO/SnO₂ nanocomposite synthesized by one-step solvothermal process and sintering, *Sens. Actuators B: Chem.* 342 (2021), 130018.
- Z. Wang, S. Gao, T. Fei, S. Liu, T. Zhang, Construction of ZnO/SnO₂ heterostructure on reduced graphene oxide for enhanced nitrogen dioxide sensitive performances at room temperature, *ACS Sens.* 4 (2019) 2048–2057.
- H. Zeng, T. Takahashi, M. Kanai, G. Zhang, Y. He, K. Nagashima, T. Yanagida, Long-term stability of oxide nanowire sensors via heavily doped oxide contact, *ACS Sens.* 2 (2017) 1854–1859.
- Y. Ren, X. Zhou, W. Luo, P. Xu, Y. Zhu, X. Li, X. Cheng, Y. Deng, D. Zhao, Amphiphilic block copolymer templated synthesis of mesoporous indium oxides with nanosheet-assembled pore walls, *Chem. Mater.* 28 (2016) 7997–8005.
- T. Ueda, I. Boehme, T. Hyodo, Y. Shimizu, U. Weimar, N. Barsan, Effects of gas adsorption properties of an Au-loaded porous In₂O₃ sensor on NO₂-sensing properties, *ACS Sens.* 6 (2021) 4019–4028.
- Z. Dong, S. Liu, In₂O₃-decorated ordered mesoporous NiO for enhanced NO₂ sensing at room temperature, *J. Mater. Sci.: Mater. Electron.* 29 (2017) 2645–2653.
- R.L. Wilson, C.E. Simion, A. Stanoiu, A. Taylor, S. Guldin, J.A. Covington, C. J. Carmalt, C.S. Blackman, Humidity-tolerant ultrathin NiO gas-sensing films, *ACS Sens.* 5 (2020) 1389–1397.
- H. Fang, S. Li, H. Zhao, J. Deng, D. Wang, J. Li, Enhanced NO₂ gas sensing performance by hierarchical CuO-Co₃O₄ spheres, *Sens. Actuators B: Chem.* 352 (2022), 131068.
- P. Sun, Y. Cao, J. Liu, Y. Sun, J. Ma, G. Lu, Dispersive SnO₂ nanosheets: Hydrothermal synthesis and gas-sensing properties, *Sens. Actuators B: Chem.* 156 (2011) 779–783.
- Q. Qin, Y. Li, W. Bu, L. Meng, X. Chuai, Z. Zhou, C. Hu, Self-template-derived ZnCo₂O₄ porous microspheres decorated by Ag nanoparticles and their selective detection of formaldehyde, *Inorg. Chem. Front.* 8 (2021) 811–820.
- N. Saito, H. Haneda, K. Watanabe, K. Shimano, I. Sakaguchi, Highly sensitive isoprene gas sensor using Au-loaded pyramid-shaped ZnO particles, *Sens. Actuators B: Chem.* 326 (2021), 128999.
- C. Wang, Y. Zhang, X. Sun, Y. Sun, F. Liu, X. Yan, C. Wang, P. Sun, G. Lu, Preparation of Pd/PdO loaded WO₃ microspheres for H₂S detection, *Sens. Actuators B: Chem.* 321 (2020), 128629.
- H. Wang, Y. Li, C. Wang, Y. Li, J. Bai, Y. Liu, L. Zhou, F. Liu, K. Shimano, G. Lu, N-pentanol sensor based on ZnO nanorods functionalized with Au catalysts, *Sens. Actuators B: Chem.* 339 (2021), 129888.
- P. Wang, T. Dong, C. Jia, P. Yang, Ultrasensitive acetone-gas sensor based ZnO flowers functionalized by Au nanoparticle loading on certain facet, *Sens. Actuators B: Chem.* 288 (2019) 1–11.
- A. Yu, Z. Li, J. Yi, Selective detection of parts-per-billion H₂S with Pt-decorated ZnO nanorods, *Sens. Actuators B: Chem.* 333 (2021), 129545.
- Y. Zhao, S. Wang, W. Yuan, S. Fan, Z. Hua, Y. Wu, X. Tian, Selective detection of methane by Pd-In₂O₃ sensors with a catalyst filter film, *Sens. Actuators B: Chem.* 328 (2021), 129030.
- J. Zhao, W. Wang, Y. Liu, J. Ma, X. Li, Y. Du, G. Lu, Ordered mesoporous Pd/SnO₂ synthesized by a nanocasting route for high hydrogen sensing performance, *Sens. Actuators B: Chem.* 160 (2011) 604–608.
- X. Wang, J. Lu, W. Han, J. Yang, B. Jiang, Y. Sun, H. Zhang, G. Lu, Co-PBA MOF-derived hierarchical hollow Co₃O₄@NiO microcubes functionalized with Pt for superior H₂S sensing, *Sens. Actuators B: Chem.* 342 (2021), 130028.
- X. Yang, Q. Yu, S. Zhang, P. Sun, H. Lu, X. Yan, F. Liu, X. Zhou, X. Liang, Y. Gao, G. Lu, Highly sensitive and selective triethylamine gas sensor based on porous SnO₂/Zn₂SnO₄ composites, *Sens. Actuators B: Chem.* 266 (2018) 213–220.
- F. Gu, M. Di, D. Han, S. Hong, Z. Wang, Atomically dispersed Au on In₂O₃ nanosheets for highly sensitive and selective detection of formaldehyde, *ACS Sens.* 5 (2020) 2611–2619.
- Z. Yang, Y. Zhang, L. Zhao, T. Fei, S. Liu, T. Zhang, The synergistic effects of oxygen vacancy engineering and surface gold decoration on commercial SnO₂ for ppb-level DMMP sensing, *J. Colloid Interface Sci.* 608 (2022) 2703–2717.
- E. Leblanc, L. Perier-Camby, G. Thomas, R. Gibert, M. Primet, P. Gelin, NO_x adsorption onto dehydroxylated or hydroxylated tin dioxide surface. Application to SnO₂-based sensors, *Sens. Actuators B: Chem.* 62 (2000) 67–72.
- J. Bai, Y. Luo, C. Chen, Y. Deng, X. Cheng, B. An, Q. Wang, J. Li, J. Zhou, Y. Wang, E. Xie, Functionalization of 1D In₂O₃ nanotubes with abundant oxygen vacancies by rare earth dopant for ultra-high sensitive ethanol detection, *Sens. Actuators B: Chem.* 324 (2020), 128755.
- J. Yang, B. Jiang, X. Wang, C. Wang, Y. Sun, H. Zhang, K. Shimano, G. Lu, MOF-derived porous NiO/NiFe₂O₄ nanocubes for improving the acetone detection, *Sens. Actuators B: Chem.* 366 (2022), 131985.
- M.H. Raza, K. Movlaee, S.G. Leonardi, N. Barsan, G. Neri, N. Pinna, Gas sensing of NiO-SCCNT core-shell heterostructures: optimization by radial modulation of the hole-accumulation layer, *Adv. Funct. Mater.* 30 (2020), 1906874.
- K. Kim, J.K. Park, J. Lee, Y.J. Kwon, H. Choi, S.M. Yang, J.H. Lee, Y.K. Jeong, Synergistic approach to simultaneously improve response and humidity-independence of metal-oxide gas sensors, *J. Hazard. Mater.* 424 (2022), 127524.
- N. Yamazoe, K. Suematsu, K. Shimano, Two types of moisture effects on the receptor function of neat tin oxide gas sensor to oxygen, *Sens. Actuators B: Chem.* 176 (2013) 443–452.
- R.G. Pavelko, H. Daly, C. Hardacre, A.A. Vasiliev, E. Llobet, Interaction of water, hydrogen and their mixtures with SnO₂ based materials: The role of surface hydroxyl groups in detection mechanisms, *Phys. Chem. Chem. Phys.* 12 (2010) 2639–2647.
- J. Yang, W. Han, J. Ma, C. Wang, K. Shimano, S. Zhang, Y. Sun, P. Cheng, Y. Wang, H. Zhang, G. Lu, Sn doping effect on NiO hollow nanofibers based gas

sensors about the humidity dependence for triethylamine detection, *Sens. Actuators B: Chem.* 340 (2021), 129971.

- [40] O. Sisman, N. Poli, D. Zappa, E. Comini, Synthesis of nanoporous TiO₂ with the use of diluted hydrogen peroxide solution and its application in gas sensing, *Coatings* 9 (2019) 681.
- [41] Z.P. Tshabalala, T.P. Mokoena, M. Jozela, J. Tshilongo, T.K. Hillie, H.C. Swart, D. E. Motaung, TiO₂ nanowires for humidity-stable gas sensors for toluene and xylene, *ACS Appl. Nano Mater.* 4 (2020) 702–716.
- [42] M. Lei, M. Gao, X. Yang, Y. Zou, A. Alghamdi, Y. Ren, Y. Deng, Size-controlled Au nanoparticles incorporating mesoporous ZnO for sensitive ethanol sensing, *ACS Appl. Mater. Interfaces* 13 (2021) 51933–51944.
- [43] H.J. Kim, J.H. Lee, Highly sensitive and selective gas sensors using p-type oxide semiconductors: Overview, *Sens. Actuators B: Chem.* 192 (2014) 607–627.
- [44] Y. Zhang, Z. Yang, L. Zhao, T. Fei, S. Liu, T. Zhang, Boosting room-temperature ppb-level NO₂ sensing over reduced graphene oxide by co-decoration of alpha-Fe₂O₃ and SnO₂ nanocrystals, *J. Colloid Interface Sci.* 612 (2022) 689–700.
- [45] D. Degler, S. Rank, S. Müller, H.W. Pereira de Carvalho, J.-D. Grunwaldt, U. Weimar, N. Barsan, Gold-loaded Tin dioxide gas sensing materials: Mechanistic insights and the role of gold dispersion, *ACS Sens.* 1 (2016) 1322–1329.
- [46] Z. Yang, D. Zhang, D. Wang, Carbon monoxide gas sensing properties of metal-organic frameworks-derived tin dioxide nanoparticles/molybdenum diselenide nanoflowers, *Sens. Actuators B: Chem.* 304 (2020), 127369.
- [47] D. Zhang, Z. Yang, P. Li, M. Pang, Q. Xue, Flexible self-powered high-performance ammonia sensor based on Au-decorated MoSe₂ nanoflowers driven by single layer MoS₂-flake piezoelectric nanogenerator, *Nano Energy* 65 (2019), 103974.

Weiyi Bu received his bachelor degree in 2020 in College of Electronics Science and Engineering in Jilin University, China. He is currently studying for degree of PhD in College of Electronic Science and Engineering at Jilin University, China. His work is studying the development of single atom catalysts loaded metal oxide semiconductor gas sensors.

Yan zhang received the bachelor degree in Yangtze University in 2021. He is currently studying for his degree of master in College of Electronic Science and Engineering, Jilin University, China.

Qixuan Qin received his BS, MS degree from the College of Electronics Science and Engineering, Jilin University, China in 2015 and 2019, respectively. He entered the PhD course in 2019, majored in development of spinel structure metal oxide semiconductor gas sensors.

Yuliang Li received his bachelor degree in 2019 in College of Electronics Science and Engineering in Jilin University, China. He is currently studying for his degree of master in College of Electronic Science and Engineering, Jilin University, China.

Xiaohong Chuai received the Ph. D degree in inorganic nonmetal science from Beijing University of science in 2001, and then worked at the school of Electronic Science and engineering, Jilin University. Now, she is engaged in the synthesis and characterization of the semiconducting functional materials and gas sensors.

Zhijie Zhou received the B.Eng. and M.Eng. degrees from the High-Tech Institute of Xi'an, Xi'an, China, in 2001 and 2004, respectively, and the Ph.D. degree from Tsinghua University, Beijing, China, in 2010. He is currently a professor with the High-Tech Institute of Xi'an. He was also a Post-Doctoral Fellow with the Department of Information and Control Engineering, Xi'an University of Technology, Xi'an, from 2014 to 2017. His current research interests include belief rule base, complex system modeling, and health management.

Changhua Hu received the B.Eng. and M.Eng. degrees from the High-Tech Institute of Xi'an, Xi'an, China, in 1987 and 1990, respectively, and the Ph.D. degree from the North Western Polytechnic University, Xi'an, in 1996. He is currently a professor with the High-Tech Institute of Xi'an. His research interests include fault diagnosis, residual life prediction, and fault-tolerant control.

Tianshuang Wang received his PhD degree from the Electronic Science and Engineering department, Jilin University, China in 2020. Presently, he is a post-doctor and interested in the synthesis and characterization of the semiconducting functional materials and gas sensors.

Peng Sun received his PhD degree from the Electronics Science and Engineering department, Jilin University, China in 2014. Now, he is engaged in the synthesis and characterization of the semiconducting functional materials and gas sensors.

Fangmeng Liu received his PhD degree in 2017 from College of Electronic Science and Engineering, Jilin University, China. Now he is an associate professor of Jilin University, China. His current research interests include the application of functional materials and development of solid-state electrolyte gas sensor and flexible device.

Geyu Lu received the B. Eng. degree in Electronic Sciences in 1985 and the M. Eng. degree in 1988 from Jilin University in China and the Dr. Eng. degree in 1998 from Kyushu University in Japan. Now he is a professor of Jilin University, China. His current research interests include the development of chemical sensors and the application of the function materials.